Title

Structural and functional conservation of key domains in InsP3 and ryanodine receptors

Journal

Nature, 483(7387)

ISSN

0028-0836

Authors

Seo, Min-Duk
Velamakanni, Saroj
Ishiyama, Noboru
et al.

Publication Date

2012-03-01

DOI

10.1038/nature10751

Peer reviewed

Published in final edited form as:
Nature. ; 483(7387): 108–112. doi:10.1038/nature10751.

Structural and functional conservation of key domains in $InsP_3$ and ryanodine receptors

Min-Duk Seo[1,*], **Saroj Velamakanni**[2,*], **Noboru Ishiyama**[1], **Peter B. Stathopulos**[1], **Ana M. Rossi**[2], **Samir A. Khan**[2], **Philippa Dale**[2], **Congmin Li**[3], **James B. Ames**[3], **Mitsuhiko Ikura**[1], and **Colin W. Taylor**[2]

[1]Ontario Cancer Institute and Department of Medical Biophysics, University of Toronto, Ontario, M5G 1L7, Canada

[2]Department of Pharmacology, University of Cambridge, Tennis Court Road, Cambridge, CB2 1PD, UK

[3]Department of Chemistry, University of California, Davis, California, 95616, USA

Abstract

Inositol 1,4,5-trisphosphate receptors ($InsP_3R$) and ryanodine receptors (RyR) are tetrameric intracellular Ca^{2+} channels[1]. For each, the pore is formed by C-terminal transmembrane domains and regulated by signals detected by the large cytosolic structures. $InsP_3R$ gating is initiated by $InsP_3$ binding to the $InsP_3$-binding core (IBC, residues 224-604 of $InsP_3R1$)[2] and it requires the suppressor domain (SD, residues 1-223)[2-8]. We present structures of the N-terminal region (NT) of $InsP_3R1$ with (3.6 Å) and without (3.0 Å) $InsP_3$ bound. The arrangement of the three NT domains, the SD, IBC-β and IBC-α, identifies two discrete interfaces (α and β) between the IBC and SD. Similar interfaces occur between equivalent domains (A, B and C) in RyR1[9]. The orientations of the three domains docked into a tetrameric structure of $InsP_3R$[10] and of the ABC domains in RyR[9] are remarkably similar. The importance of the α-interface for activation of $InsP_3R$ and RyR is confirmed by mutagenesis and, for RyR, by disease-causing mutations[9,11,12]. $InsP_3$ causes partial closure of the clam-like IBC, disrupting the β-interface and pulling the SD towards the IBC. This reorients an exposed SD loop (HS-loop) that is essential for $InsP_3R$ activation[7]. The loop is conserved in RyR and includes mutations associated with malignant hyperthermia and central core disease[9,11,12]. The HS-loop interacts with an adjacent NT, suggesting that activation re-arranges inter-subunit interactions. The A-domain of RyR functionally replaced the SD in a full-length $InsP_3R$, and an $InsP_3R$ in which its C-terminal transmembrane region was replaced by that from RyR1 was gated by $InsP_3$ and blocked by ryanodine. Activation mechanisms are conserved between $InsP_3R$ and RyR. Allosteric modulation of two similar domain interfaces within an N-terminal subunit re-orients the first domain (SD or A-domain), allowing it, via interactions of the second domain of an adjacent subunit (IBC-β or B-domain), to gate the pore.

Correspondence and requests for materials should be addressed to C.W.T (cwt1000@cam.ac.uk) or M.I. (mikura@uhnres.utoronto.ca)..
*These authors contributed equally.

Author Information The atomic coordinates of $NT^{Cysless}$ of rat $InsP_3R1$ with (3UJ4) and without $InsP_3$ bound (3UJ0) have been deposited in the Protein Data Bank. The authors declare no competing financial interests.

Full Methods and associated references are available in the online version of the paper.

Supplementary Information is linked to the online version of the paper.

Author Contributions M.S., N.I., P.B.S., M.I. and C.L. determined and analysed the structure of NT. S.V. prepared and characterized the full-length $InsP_3R$ and chimeras. A.M.R., S.A.K. and P.D. completed analyses of $InsP_3$ binding and related molecular biology. J.B.A., M.I. and C.W.T. supervised work in their respective laboratories, coordinated the project and, with input from other authors, wrote the paper.

Europe PMC Funders Author Manuscripts

The essential role of the SD in linking $InsP_3$ binding to $InsP_3R$ gating highlights the need to define the structural consequences of $InsP_3$ binding to the NT (residues 1-604 of $InsP_3R1$) (Supplementary Fig. 1). Because our attempts to crystallize the NT yielded poorly diffracting crystals, we expressed a Cys-less form of the NT ($NT^{Cysless}$). Native and Cys-less forms of the NT and IBC behaved indistinguishably (Supplementary Fig. 2 and Supplementary Tables 1-2), but $NT^{Cysless}$ provided crystals with much improved diffraction (Supplementary Table 3). We determined crystal structures of $NT^{Cysless}$ with (3.6 Å) and without (3.0 Å) $InsP_3$ bound, showing three subdomains: the SD, IBC-β (residues 224-436) and IBC-α (residues 437-604) (Fig. 1a). The structures of these subdomains were nearly identical to those of isolated native SD and IBC[2,3] (Supplementary Fig. 3).

The SD, IBC-β and IBC-α form a triangular structure, with the SD behind the $InsP_3$-binding site (Fig. 1a). The SD interacts via two interfaces with the IBC, one with IBC-β (β-interface) and another with IBC-α (α-interface). A 3^{10}-like turn between the last strand of the SD and the first strand of IBC-β positions the IBC relative to the SD (Supplementary Fig. 4e). Within this connecting turn, a salt bridge (K225/D228) stabilizes the backbone conformation and so positions residues that form the β-interface. These interactions in the connecting turn and β-interface are augmented by a network of hydrophobic interactions within IBC-β (Fig. 1b). The α-interface forms a long 'Velcro'-like structure that also involves a network of hydrophobic and electrostatic interactions (Fig. 1c). Intimate hydrophobic interactions between V33, and to a lesser extent L32, from the SD; and V452, F445, A449 and L476 from IBC-α are supported by bidentate salt bridges between R54/K127 in the SD and D444 in IBC-α (Fig. 1c). The V33K mutation at the α-interface almost abolished inhibition of $InsP_3$ binding by the SD[3,4] and reduced channel open probability[4], confirming its importance. Mutation of neighbouring residues that contribute less to the α-interface (L32K, D34K, R36E, K127E) had lesser effects on $InsP_3$ binding, while mutation of residues that do not contribute to the interface (D35K, K52E) had no effect (Supplementary Table 4)[3,4]. Hydrophobic and electrostatic interaction networks at the α- and β-interfaces contribute to a buried surface between the SD and IBC (~2040 $Å^2$) that forms a hub connecting $InsP_3$ binding to channel activation.

The structure of the NT is remarkably similar to that of the N-terminal of RyR1[9]. The three NT domains of $InsP_3R1$ (SD, IBC-β and IBC-α) can be individually superposed to corresponding domains of RyR1 (A, B and C) (Supplementary Fig. 3), and the relative orientation of the domains is nearly identical (Fig. 1d). Mutation of Y167A, located on an exposed loop of the SD opposite the IBC interfaces ('HS-loop'[11], residues 165-180, boxed in Fig. 1d), attenuates $InsP_3$-evoked Ca^{2+} release[8]; and Ca^{2+}, a co-regulator of $InsP_3R$[14], causes the loop to become accessible.[15] The disease-associated 'hot spot loop' of RyR1[11] sits at the same location within the ABC structure[9] (Fig. 1d) and a mimetic peptide causes RyR2 to become leaky[16]. Furthermore, the backbone and side chain conformation of this loop region superposes well in the two receptors (Fig. 1e). The HS-loop provides a critical link between $InsP_3$ binding and gating.

The domain interfaces of $InsP_3R1$-NT and RyR1-ABC are also similar. The bidentate salt bridges between R54/K127 and D444 at the $InsP_3R1$ α-interface are preserved in RyR1 ABC, albeit in a reversed-charge manner between D40/D61 and R402 (Supplementary Fig. 4a). In RyR1, mutation of these residues (R402C, D61N) is associated with malignant hyperthermia and central core disease[9], suggesting that disruption of the interaction perturbs RyR gating, as it does for $InsP_3R$. The structural similarities extend also to the β-interface of $InsP_3R1$ and corresponding A/B interface in RyR1 (Supplementary Fig. 4b-d).

Our structures of $NT^{Cysless}$ with and without $InsP_3$ bound, together with that of the $InsP_3$-bound IBC[2] (Supplementary Fig. 5) reveal the structural changes evoked by $InsP_3$ (Fig. 2). Side chains of nine residues become organized around $InsP_3$ (Supplementary Fig. 5a), and the domain orientation angle between IBC-β and IBC-α is reduced (by ~8°) after $InsP_3$ binding (Fig. 2 and Supplementary Fig. 5a). This $InsP_3$-evoked 'clam closure', which is consistent with earlier predictions[17] and small-angle X-ray scattering[18], causes the distance across the entrance to the $InsP_3$-binding pocket to decrease (Supplementary Fig. 5b, c). A similar agonist-evoked domain closure occurs in some glutamate receptor channels[19]. The SD and IBC remain associated after closure of the IBC (Fig. 2). $InsP_3$ binding hardly changes the interactions across the extensive α-interface, but at the β-interface the SD residues move away from IBC-β (Supplementary Fig. 5d-f). With the SD glued to IBC-α by the α-interface, and the β-interface serving as a lubricant, $InsP_3$ binding causes the SD to twist (by ~9°) and move closer to the top of the IBC (Fig. 2). This causes an amplified translational movement of the conserved HS-loop in the SD (Supplementary Fig. 5g). While our work was under review, 3.8 Å structures of apo- and $InsP_3$-bound NT derived from a single crystal grown in excess $InsP_3$ were published, showing similar $InsP_3$-induced allostery in the interfaces between domains[13]. This confirms our observations, but our higher resolution structures reveal more detail of the α- and β-interfaces associated with this conformational change (Supplementary Discussion).

Docking the ABC structure into cryo-EM maps of RyR1 showed that the N-terminal domains form a central ring at the top of the mushroom-like RyR1[9]. Rigid-body docking of our apo-$NT^{Cysless}$ structure into a cryo-EM 10 Å structure of a closed $InsP_3R1$[10] reveals an arrangement remarkably similar to that of RyR1 with a high docking contrast (Fig. 3 and Supplementary Fig. 6). The three domains of the four NTs, which form the upper cytoplasmic surface of the mushroom-like $InsP_3R$, are arranged as four hillocks around a central bowl. This arrangement allows $InsP_3$ unrestricted access to the IBC from the side of the cap (Fig. 3), and it is consistent with accessibility studies and binding sites for regulatory proteins (Supplementary Fig. 6c and Supplementary Table 5). Within the tetrameric $InsP_3R$, the only contacts between NT subunits are via the critical HS-loop of the SD and a flexible loop (β20-β21, Supplementary Fig. 7) in IBC-β (Fig. 3c, d). The latter is longer in RyR and it lies ~10 Å further from the neighbouring hot spot loop[9] (Fig. 3c, d). In $InsP_3R$, the arm domains (residues 67-109) of each SD are the only NT structures that extend beyond the cap towards the pore (Fig. 3a), but these domains are neither essential for $InsP_3R$ activation[8] nor conserved in RyR[9,11].

The structural similarities between the N-termini of RyR and $InsP_3R$ prompted us to examine whether the domains are functionally interchangeable. In a chimeric N-terminal fragment comprising the A-domain of RyR2 and IBC from $InsP_3R1$ (RyR2A-IBC), the A-domain mimicked the SD by inhibiting $InsP_3$ binding (Fig. 4a, b). Mutations within the A-domain loop that forms the A-B interface in RyR[9] or the equivalent $InsP_3R$ loop in the SD attenuated this inhibition of binding (Fig. 4c, Supplementary Table 6 and Supplementary Fig. 8). $InsP_3$ stimulated Ca^{2+} release via $InsP_3R1$ or a chimeric $InsP_3R1$ in which the SD was replaced by the A-domain of RyR1 (RyR1A-$InsP_3R1$ (Fig. 4a, d and Supplementary Fig. 9). Both $InsP_3Rs$ were similarly expressed and they released similar fractions of the Ca^{2+} stores and with similar sensitivity to $InsP_3$ (Supplementary Table 7). Opening of native $InsP_3R$ or RyR is restrained by interactions between cytosolic domains[20,21]. It is therefore significant that expression of $InsP_3R1$ or RyR1A-$InsP_3R1$ affected neither the Ca^{2+} content of the ER nor the Ca^{2+} leak from it (Supplementary Fig. 10), confirming that $InsP_3R$ and RyR1A-$InsP_3R1$ have no detectable spontaneous activity. This demonstrates that the SD of $InsP_3R$ can be functionally substituted by the A-domain of RyR.

An $InsP_3R1$ in which residues downstream of TMD1 were replaced by the equivalent region of RyR1 ($InsP_3R1$-RyR1) also responded to $InsP_3$ (Fig. 4a,e). Expression of $InsP_3R1$-RyR1 increased Ca^{2+} leak from the ER, and this was reversed by ryanodine, which blocks the RyR pore[22]. However, the increased leak was insufficient to affect the steady-state Ca^{2+} content (Supplementary Fig. 10), suggesting that $InsP_3R1$-RyR1 has minimal spontaneous activity. Expression of $InsP_3R1$-RyR1 matched that of other $InsP_3Rs$, but cells expressing $InsP_3R1$-RyR1 were ~20-fold less sensitive to $InsP_3$ (Supplementary Table 7). Because the TMDs minimally affect $InsP_3$ binding[23], this diminished response probably reflects a decrease in $InsP_3$ efficacy. The increased Ca^{2+} leak and reduced efficacy of $InsP_3$ suggest that within $InsP_3R1$-RyR, communication between the SD and channel are slightly less effective than in native $InsP_3R$. Nevertheless, it is remarkable that cytosolic domains of an $InsP_3R$ should so effectively regulate the pore of a RyR when the two receptors share only modest sequence identity and differ in the number of residues separating the NT from TMDs (Fig. 4a), and in the lengths and sequences of their C-terminal tails and the loops linking TMDs (Supplementary Fig. 11).

Ryanodine (10 μM) had no effect on $InsP_3R1$ or RyR1A-$InsP_3R$, but it abolished $InsP_3$-evoked Ca^{2+} release via $InsP_3R1$-RyR1 (Fig. 4e, f). Because ryanodine binds selectively to active RyR[24], ^{3}H-ryanodine binding is stimulated by agonists of RyR, like caffeine. Whereas caffeine had no effect on specific ^{3}H-ryanodine binding to $InsP_3R1$-RyR1, $InsP_3$ stimulated it (Fig. 4g). $InsP_3$ therefore causes conformational changes to the channel of $InsP_3R1$-RyR1 that mimic those of native RyR in allowing binding of ^{3}H-ryanodine.

Conservation of structure-function relationships between $InsP_3R$ and RyR (Fig. 1-4) allows comparisons between them to suggest possible mechanisms of $InsP_3R$ activation. For both receptors, gating requires that conformational changes in the large cytoplasmic structures pass to the TMDs[10,22], but the N-terminal domains of $InsP_3R$ and RyR are at least 60 Å from these TMDs[1,9,22] (Fig. 3a and Supplementary Fig. 6). Despite some evidence implicating direct interactions between the SD and TMD4-5 loop in gating $InsP_3R$ (Supplementary Discussion), we suggest, and in keeping with results from RyR[20,26,27], that additional cytosolic domains couple the NT to opening of the pore. The exposed HS-loop in the SD (Fig. 1d and 3c,d) (hot spot-loop of RyR)[9,11] is arranged similarly within the isolated N-terminal structures of $InsP_3R$ and RyR (Fig. 1d) and it reorients after $InsP_3$ binding (Fig. 2). When the NT is docked into the $InsP_3R$ structure[10], the HS-loop forms (with an exposed loop of IBC-β) the only interface between adjacent NT, however, the equivalent loop is displaced in the RyR[9] (Fig. 3c, d). $InsP_3$ binding closes the clam-like IBC, disrupting the β-interface and re-orienting the HS-loop (Fig. 2 and Supplementary Fig. 5). This, we suggest, disrupts interaction of the HS-loop with a neighbouring NT to cause a coordinated re-arrangement of the apical $InsP_3R$ structure (Fig. 3). The open state of RyR1 is associated with outward movement of protein density in regions that match the locations of docked ABC structures[9,22] and with larger movements of peripheral 'clamp domains'[9,22] that are absent from $InsP_3R$[10]. Movement of these apical domains in RyR is accompanied by re-arrangements within regions that taper towards the pore[22] and which, in $InsP_3R$, include the most flexible parts of its structure[10]. We suggest that similar rearrangements of the apical surface of $InsP_3R$ and RyR couple by shared mechanisms to additional cytosolic domains to gate the pore of each channel.

METHODS SUMMARY

The N-terminal (NT, residues 1-604) of rat $InsP_3R1$ in which all Cys were replaced by Ala ($NT^{Cysless}$) was expressed in *E. coli* and purified. Crystals of $NT^{Cysless}$ were grown by the hanging-drop vapour diffusion method in 0.1 M Hepes pH 7.0, 0.8-1.0 M $(NH_4)_2SO_4$, and 3% (v/v) trimethylamine N-oxide for apo-state crystals, or 0.1 M Na citrate (pH 6.0), 8% (w/

v) PEG-6000, 70 mM Li_2SO_4, 3% dimethyl sulfoxide for $InsP_3$-bound crystals. Diffraction data were collected at 100 K on the 19-ID (apo-crystals) or 19-BM ($InsP_3$-bound crystals) beam lines at the Advanced Photon Source Synchrotron facility (Argonne, IL) and processed with HKL2000[28]. Structures of apo-$NT^{Cysless}$ at 3.0 Å resolution and $InsP_3$-bound $NT^{Cysless}$ at 3.6 Å resolution were determined by molecular replacement using structures of the SD (PDB code: 1XZZ)[3] and the IBC (1N4K)[2] as search models with the program Phaser[29]. Iterative refinement and model building were performed with Refmac5 and Coot, respectively. Numbering of secondary structure motifs is in accord with Supplementary Figure 7. Binding of ^{3}H-$InsP_3$ or ^{3}H-ryanodine to full-length $InsP_3R1$, chimeras of $InsP_3R1$ and RyR, and to related N-terminal fragments was defined using equilibrium-competition binding assays[4]. Functional properties of $InsP_3R1$ and chimeras were characterized after stable expression in DT40 cells lacking endogenous $InsP_3R$[4]. A luminal Ca^{2+} indicator was used to record $InsP_3$-evoked Ca^{2+} release from the intracellular stores of permeabilized DT40 cells[4].

Supplementary Material

Refer to Web version on PubMed Central for supplementary material.

Acknowledgments

We thank Paul Allen (Harvard University) and David MacLennan (University of Toronto) for kind gifts of plasmids encoding RyR2 and RyR1, respectively. C.W.T. thanks Taufiq Rahman and Vera Konieczny (University of Cambridge) for discussions. M.I. acknowledges Katsuhiko Mikoshiba and Takayuki Michikawa (RIKEN) for long-standing support and discussions. This work was supported by grants from the Heart and Stroke Foundation of Ontario (T-7181) to M.I., and the Wellcome Trust (085295), Biotechnology and Biological Sciences Research Council (BB/H009736) and Medical Research Council (G0900049) to C.W.T. M.S. is supported by postdoctoral fellowships from the Canadian Institutes of Health Research and the National Research Foundation of Korea (2009-352-E00006). A.M.R. is a fellow of Queens' College, Cambridge. M.I. holds a Canadian Research Chair in Cancer Structural Biology.

Appendix

METHODS

Materials

$InsP_3$ was from Enzo Life Sciences (Exeter, UK). Adenophostin A was from A. G. Scientific (San Diego, CA, USA). Ryanodine was from Ascent Scientific (Bristol, UK). Cyclopiazonic acid was from Sigma (St. Louis, MO). Sources of other materials are specified in earlier publications[2-4,18] or in the descriptions that follow.

Cloning, expression and purification of N-terminal fragments of $InsP_3R1$ and RyR2

The open reading frame (ORF) encoding the N-terminal fragment (NT, residues 1-604) of rat $InsP_3R1$ (GenBank: GQ233032.1) was amplified by PCR from the full-length clone lacking the S1 splice site using forward 5′-CGGGATCCATGTCTGACAAAATGTCTAGT-3′ and reverse 5′-CGCGCTCGAGTCACTTTCGGTTGTTGTGGA-3′ primers. The PCR product was ligated into a pGEX-6P-2 vector (GE Healthcare, Little Chalfont, Bucks, UK) as a BamHI/XhoI fragment to give pGEX(NT), which includes an N-terminal GST tag followed by a PreScission-cleavage site. To generate $NT^{Cysless}$, a QuikChange multisite directed mutagenesis kit (Agilent, Stockport, UK) was used to mutate all Cys residues to Ala using pGEX-6P-2-(NT) as the template and the primers listed in Supplementary Table 8. Residues are numbered by reference to rat $InsP_3R1$ containing the S1 splice site.

Plasmids encoding GST-tagged IBC (residues 224-604) and $IBC^{Cysless}$ were generated using PCR to amplify the appropriate sequence from the ORF of full-length rat $InsP_3R1$ or $NT^{Cysless}$ using the following primers: forward 5′-CGGGATCCATGAAATGGAGTAACAAAG-3′ and reverse 5′-CGCGCTCGAGTCACTTTCGGTTGTTGTGGA-3′. Each PCR product was ligated into a pGEX-6P-2 vector as a BamHI/Xho I fragment to produce pGEX-6P-2-(IBC) and pGEX-6P-2-($IBC^{Cysless}$), respectively. For analysis of the effects of mutations within the SD on $InsP_3$ binding, the plasmids described previously were used to express His_6-tagged NT and IBC[4] and the His_6-tag was cleaved prior to experiments[4]. Mutations were introduced using a QuikChange mutagenesis kit and the primers listed previously[4] or in Supplementary Table 9.

The sequence encoding the A-domain of RyR2 was amplified by PCR from rabbit RyR2 (GenBank: GI164831)[30] in pcDNA3 using the following primers: forward 5′-ACTAGTCTCGAGGTGCTCTTCCAGGGGCCCATGGCTGATGGGGGCGAA-3′ and reverse 5′-GATATCCTTCACTTCCTGAGCTGATGGG-3′. The ORF for the IBC of $InsP_3R1$ was excised from pGEX-6P-2-(NT) as a BamHI/XhoI fragment and ligated into a pET41a vector to produce pET41a-(IBC). To generate a plasmid encoding a chimeric NT in which the A-domain of RyR2 (residues 1-210) was fused to the IBC of $InsP_3R1$ (residues 225-604) (RyR2A-IBC), the PCR product from above was ligated into pET41a-(IBC) as a SpeI/EcoRV fragment to produce pet41a-(RyR2A-IBC). Mutations within the ORF of the A-domain of RyR2A-IBC were generated by site-directed mutagenesis using the QuikChange Lightning mutagenesis kit (Stratagene) using the primers listed in Supplementary Table 9. The complete coding sequences of all constructs were confirmed by sequencing. The sequences of the proteins used are summarized in Supplementary Table 1 and Figure 4a.

For structural studies, $NT^{Cysless}$ was expressed as a GST-fusion protein in BL21-CodonPlus(DE3) *E. coli* strain. Transformed cells were first grown at 37°C until the OD_{600} reached ~1.0 and then induced with 0.5 mM IPTG at 15°C for ~18 h. Proteins were purified using glutathione sepharose 4B resin (GE Healthcare), and the GST tag was cleaved from the eluted proteins with PreScission protease (GE Healthcare) during overnight dialysis at 4°C in cutting buffer (20 mM Tris-HCl, pH 8.4, 300 mM NaCl, 5% glycerol, 2 mM DTT). The cleaved proteins were further purified with cation-exchange chromatography (Fractogel EMD SO3-resin, EM Industries Inc.) followed by size-exclusion chromatography (Superdex 200, GE Healthcare). Purified proteins were concentrated to 14 mg/ml in a buffer comprising 20 mM Tris-HCl, pH 8.4, 360 mM NaCl, 2.5% glycerol, 0.2 mM TCEP, 1 mM PMSF. Similar methods were used to express $InsP_3R$ fragments for binding studies, but with the following modifications: bacteria were initially grown at 22°C, the GST-tag was cleaved by incubation of bacterial lysates immobilized on glutathione sepharose 4B resin with PreScission for 5 h in PreScission-cleavage buffer (GE Healthcare). The eluant was then used for ^3H-$InsP_3$ binding analyses without further purification. Western blotting and silver-stained gels were used to verify expression and purification of NT fragments.

Western blotting

Western blotting of DT40 cells solubilized in TEM containing Triton-X100 (1% v/v) was performed as previously described[31] using anti-peptide antisera corresponding to residues 240-253 within the IBC (AbNT, 1:1000) or 2733-2749 (AbCT, 1:500) of rat $InsP_3R1$. The secondary antibody was HRP-conjugated donkey anti-rabbit antibody (1: 5000, Santa Cruz Biotechnology).

^{3}H-InsP_3 Binding

Equilibrium-competition binding assays were performed at 4°C in Tris-EDTA medium (TEM: 50 mM Tris, 1 mM EDTA, pH 8.3) containing ^{3}H-InsP_3 (0.75 nM, Perkin-Elmer Life Sciences), purified protein (1-4 μg) and unlabelled InsP_3 in a final volume of 500 μl. After a 5-min incubation, during which equilibrium was attained, reactions were terminated by addition of 500 μl of TEM containing 30% poly(ethylene glycol) 8000 and γ-globulin (750 μg) followed by centrifugation (20,000 *g*, 5 min). For ^{3}H-InsP_3 binding to IBC, the amount of ^{3}H-InsP_3 was reduced to 0.25 nM, and incubation volumes were doubled. Pellets were solubilized in 200 μl of TEM containing 2% Triton-X 100 (v/v), mixed with EcoScintA scintillation liquid (National Diagnostics) and radioactivity was determined by liquid scintillation counting. Non-specific binding was determined in the presence of 10 μM InsP_3. Binding results were fitted to a Hill equation (GraphPad Prism, version 5) from which pIC_{50} (-logIC_{50}, where IC_{50} is the half-maximal inhibitory concentration) and thereby pK_D (-logK_D) values were calculated[32].

^{3}H-ryanodine binding

Microsomal membranes were prepared from DT40 cells by lysis with a glass homogenizer and sonication in cytosol-like medium (CLM) supplemented with protease inhibitors (Roche complete protease inhibitor cocktail), followed by centrifugation (50,000 *g*, 30 min). CLM had the following composition: 140 mM KCl, 20 mM NaCl, 1 mM EGTA, 20 mM Pipes, 2 mM $MgCl_2$, 375 μM $CaCl_2$ (free [Ca^{2+}] ~ 220 nM), pH 7. Equilibrium-competition binding was performed with microsomal membranes (100 μg protein/ml) at 4°C in 200 μl of CLM supplemented with protease inhibitors and ^{3}H-ryanodine (100 nM, Perkin-Elmer Life Sciences). Reactions were terminated after 90 min, and radioactivity was determined as described for ^{3}H-InsP_3 binding. Non-specific binding was defined by addition of 10 μM unlabelled ryanodine.

^{3}H-ryanodine binding to RyR typically requires many hours to reach equilibrium[24] because it binds only to the open state of the channel and spontaneous openings are rare. In our analyses of ^{3}H-ryanodine binding to InsP_3R1-RyR1 (Fig. 4g) equilibrium was attained within 90 min, perhaps because the modestly increased spontaneous activity of the chimeric channel (Supplementary Fig. 10b) contributed to an increased rate of ^{3}H-ryanodine binding to the open state. In parallel comparisons, specific binding of ^{3}H-ryanodine to InsP_3R1-RyR1 expressed in DT40 cells and stimulated with InsP_3 (1 μM) was (d.p.m.; mean [range] for 2 independent experiments): 4241 [4073-4409] after 90 min, 4941 [4825-5058] after 3 h, and 4410 [4108-4712] after 14 h. It is, however, important to note that our conclusion that InsP_3 selectively stimulates ^{3}H-ryanodine binding to InsP_3R1-RyR1 is not dependent on having measured binding under equilibrium conditions.

Crystallization and data collection

Crystals of apo-$NT^{Cysless}$ were grown by the hanging-drop vapour diffusion method at 293 K by mixing 1 μl of protein with an equal volume of reservoir solution (0.1 M Hepes, pH 7.0, 0.8-1.0 M $(NH_4)_2SO_4$). Using an additives screen, 3% (v/v) trimethylamine N-oxide was identified as an important additive to obtain single rod-shaped crystals. After a series of microseeding trials, rod-shaped single crystals were obtained within 5 days. For crystallization of InsP_3-bound $NT^{Cysless}$, five molar excess of InsP_3 (~1 mM) was added before crystallization. Crystals of InsP_3-bound $NT^{Cysless}$ were grown using the same method except for the reservoir solution containing 0.1 M Na citrate (pH 6.0), 8% (w/v) PEG-6000, 70 mM Li_2SO_4 and 3% dimethyl sulfoxide.

For data collection, crystals were equilibrated in 25% glycerol cryo-protective solutions containing reservoir buffer, and flash frozen in liquid nitrogen. Diffraction data were

collected at 100K on 19-ID beam line for apo-state crystals or 19-BM beam line for $InsP_3$-bound crystals at the Advanced Photon Source Synchrotron facility (Argonne, IL), and were processed with HKL2000. Crystals of apo-$NT^{Cysless}$ belong to the space group P1 with cell dimension a=63.1 Å, b=77.2 Å, c=101.5 Å, α=105.4°, β=100.0°, γ=101.0°. Crystals of $InsP_3$-bound $NT^{Cysless}$ belong to the space group C2 with cell dimension a=189.2 Å, b=78.7 Å, c=134.1 Å, α=90.0°, β=124.5°, γ=90.0°. Crystals of both apo- and $InsP_3$-bound $NT^{Cysless}$ contained two molecules in the asymmetric unit (Supplementary Table 3).

Structure determination and refinement

Structures of apo-$NT^{Cysless}$ at 3.0 Å resolution and of $InsP_3$-bound $NT^{Cysless}$ at 3.6 Å resolution were determined by molecular replacement using structures of the SD (PDB code: 1XZZ)[3] and the IBC (PDB code: 1N4K)[2] as search models with the program Phaser[29]. Iterative refinement and model building were performed with Refmac5[33] and Coot[34], respectively (Supplementary Table 3). Structures of the two molecules in the asymmetric unit of apo-$NT^{Cysless}$ are virtually identical (rmsd value = 0.543 Å) except for a minor variation in the loop between β20 and β21 which does not affect the interpretation of our results. The low rmsd between chain A and chain B is maintained through the regions of the molecule which make up interface-α and interface-β, thus increasing the validity of our description of the 'open-clam' structure. The two molecules in the asymmetric unit of $InsP_3$-bound $NT^{Cysless}$ are more converged than those of the apo-structure (rmsd value = 0.134 Å), which also validates our description of the 'closed-clam' structure. The molecule of chain A for each state was used to generate figures, but the chain B molecule of apo-$NT^{Cysless}$ was used for the side chain of D444 in Fig. 1c. All water molecules were modeled in Coot[34]. Initially, water molecules were detected using the automatic "find waters" function in the program. A $2F_0$-F_c map was used with a sigma cut-off value of 1.0, and minimum and maximum distances to protein atoms of 2.4 and 3.2 Å, respectively. We subsequently picked additional water molecules and deleted inappropriate water molecules by manually surveying the density in Coot. After refinement, all water molecules exhibiting negative electron density due to inconsistent modeling were deleted.

Circular dichroism (CD) analysis

CD spectra were collected on a Jasco J-720 spectrometer using a 1-mm path length cuvette at 20 °C. The NT and $NT^{Cysless}$ (0.2 mg/ml) were prepared in a buffer (20 mM Tris-HCl, pH 8.4, 360 mM NaCl, 2.5% glycerol, 0.2 mM TCEP, 1 mM PMSF). CD spectra were obtained from 260 to 200 nm, with a 2-nm bandwidth, an 8-s response time, and scan speed of 50 nm/min. Data are averages of three consecutive scans.

Cloning and functional expression of chimeric $InsP_3R$

To generate the plasmid encoding a chimeric $InsP_3R1$ in which residues 2274-2748 of $InsP_3R1$ (all residues downstream of those immediately before TMD1) were replaced by the equivalent region from RyR1 (residues 4511-5037) ($InsP_3R1$-RyR1), the appropriate region of the ORF of rabbit RyR1 (GenBank: X15209)[35] was amplified by PCR from the expression vector pcDNA3.2 using the following primers: forward, 5′-CGCGGGTTCGAAGTCCCCGAGGCCCCACCAGAACCCCCC-3′, and reverse 5′-CGGGGCGTCCTCGAGTCATTAGCTCAGCTGGTCCTCGTACTGCTTGCGGAAGC-3′. The PCR product was cloned in-frame as a BstBI/XhoI fragment into a pENTR1a vector containing nucleotides 1-6822 of rat $InsP_3R1$. This construct was transferred into the Gateway-compatible expression vector, pcDNA3.2, to generate pcDNA3.2-($InsP_3R1$-RyR1). A plasmid encoding $InsP_3R$ lacking the SD was generated from ORFs for the full-length $InsP_3R1$ lacking the S1 splice site (pENTR1A($InsP_3R1$)) and the IBC (pENTR1A(IBC)). Both plasmids were digested with NheI and KpnI, and the fragment from pENTR1A(IBC) was cloned into pENTR1A($InsP_3R1$). Site-directed mutagenesis was then

used to silence 3 internal BamHI sites within this construct without affecting the coding sequence to generate the plasmid pENTR1A($InsP_3R1^{\Delta SD}$). A plasmid encoding a chimera in which the SD of $InsP_3R1$ (residues 1-224) was replaced by the A-domain of RyR1 (residues 1-210) (RyR1A-$InsP_3R$) was prepared by isolating the coding sequence for the A-domain of RyR1 by PCR from the the rabbit RyR1 ORF using the following primers: forward, 5′-GCTAGCATCATGGGTGACGGAGGA-3′ and reverse 5′-GGATCCTTCACAGCAGGAGCAGATG-3′. The PCR product was cloned as a NheI/BamHI fragment into pENTR1A($InsP_3R1^{\Delta SD}$). The complete coding sequences of all plasmids were verified by sequencing. Domain boundaries of the chimeric proteins are summarized in Supplementary Table 1.

DT40-KO cells were transfected by electroporation with linearized plasmids (10 μg DNA/10^6 cells) using the Neon (Invitrogen, Paisley, UK) or Amaxa (Lonza, Slough, UK) nucleofection systems. G418 (2 mg/ml) was used to select and amplify clones of G418-resistant cells. Stable cell lines were selected and $InsP_3R$ expression was measured by Western blotting. DT40 cells were cultured in RPMI 1640 medium with L-glutamine (Invitrogen) supplemented with 10% foetal bovine serum, 1% heat-inactivated chicken serum (both from Sigma) and 10 μM 2-mercaptoethanol at 37°C in humidified air containing 5% CO_2. Cells (~2 ×10^6 cells/ml) were passaged every 2-3 days. Similar methods were used for transient transfections with RyR1 and $InsP_3R1^{CyslessNT}$, but with 50 μg DNA/3 × 10^6 cells.

Functional analyses of $InsP_3R$ in DT40 cells

Uptake of Ca^{2+} into the intracellular stores of saponin-permeabilized DT40 cells and its release by $InsP_3$ were measured using a low-affinity Ca^{2+} indicator (Mag-fluo-4) trapped within the endoplasmic reticulum[36]. All experiments were performed at 20°C in CLM supplemented with 1.5 mM MgATP to allow active Ca^{2+} uptake. After the intracellular stores had loaded to steady-state with Ca^{2+} (~150 s), $InsP_3$ was added with thapsigargin (1 μM) to prevent further Ca^{2+} uptake (Supplementary Fig. 9). The effects of $InsP_3$ were assessed after a further 10-40 s. $InsP_3$-evoked Ca^{2+} release is expressed as a fraction of the ATP-dependent Ca^{2+} uptake. Typical experiments are shown in Supplementary Figure 9.

Structural model of RyR2A-IBC

A structural homology model of RyR2A-IBC (Fig. 4c) was produced using UCSF Chimera[37] to first superpose the backbone structures of apo-$NT^{Cysless}$ and the ABC of RyR1 (PDB, 2XOA), the only RyR subtype for which there is a complete N-terminal structure[9]. This A-domain structure of RyR1 was then used to allow superposition of the A-domain from RyR2 (PDB, 3IM5)[12], effectively achieving superposition of $NT^{Cysless}$ onto a ‘virtual’ chimera of RyR2A with RyR1BC. The predicted structure of the RyR2A-IBC was then revealed by masking the SD of $InsP_3R1$ and the BC domains of RyR1 (Fig. 4c).

Computational docking

Rigid-body docking of the apo-$NT^{Cysless}$ structure into a ~10 Å cryo-EM density map of $InsP_3R1$[10] was implemented using the six-dimensional search procedure in the Situs Program package[38]. The Laplacian filter was applied to the density maps to enhance the fitting contrast. Docking of the crystal structure of RyR1-ABC (PDB code: 2XOA) into a 9.6-Å cryo-EM density map (EMDB code: EMDB-1275)[10], as previously described[9], was repeated using the above procedure. The UCSF Chimera package[37] was used to visualize the docking results with the density maps (Fig. 3 and Supplementary Fig. 6).

References

1. Serysheva, I., editor. Structure and function of calcium release channels. Academic Press; San Diego:
2. Bosanac I, Alattia J-R, Mal TK, Chan J, Talarico S, Tong FK, Tong KI, Yoshikawa F, Furuichi T, Iwai M, Michikawa T, Mikoshiba K, Ikura M. Structure of the inositol 1,4,5-trisphosphate receptor binding core in complex with its ligand. Nature. 2002; 420:696–700. [PubMed: 12442173]
3. Bosanac I, Yamazaki H, Matsu-ura T, Michikawa M, Mikoshiba K, Ikura M. Crystal structure of the ligand binding suppressor domain of type 1 inositol 1,4,5-trisphosphate receptor. Mol. Cell. 2005; 17:193–203. [PubMed: 15664189]
4. Rossi AM, Riley AM, Tovey SC, Rahman T, Dellis O, Taylor EJA, Veresov VG, Potter BVL, Taylor CW. Synthetic partial agonists reveal key steps in IP_3 receptor activation. Nat. Chem. Biol. 2009; 5:631–639. [PubMed: 19668195]
5. Uchida K, Miyauchi H, Furuichi T, Michikawa T, Mikoshiba K. Critical regions for activation gating of the inositol 1,4,5-trisphosphate receptor. J. Biol. Chem. 2003; 278:16551–16560. [PubMed: 12621039]
6. Schug ZT, Joseph SK. The role of the S4-S5 linker and C-terminal tail in inositol 1,4,5-trisphosphate receptor function. J. Biol. Chem. 2006; 281:24431–24440. [PubMed: 16815846]
7. Chan J, Yamazaki H, Ishiyama N, Seo MD, Mal TK, Michikawa T, Mikoshiba K, Ikura M. Structural studies of inositol 1,4,5-trisphosphate receptor: coupling ligand binding to channel gating. J. Biol. Chem. 2010; 285:36092–36099. [PubMed: 20843799]
8. Yamazaki H, Chan J, Ikura M, Michikawa T, Mikoshiba K. Tyr-167/Trp-168 in type1/3 inositol 1,4,5-trisphosphate receptor mediates functional coupling between ligand binding and channel opening. J. Biol. Chem. 2010; 285:36081–36091. [PubMed: 20813840]
9. Tung CC, Lobo PA, Kimlicka L, Van Petegem F. The amino-terminal disease hotspot of ryanodine receptors forms a cytoplasmic vestibule. Nature. 2010; 585:585–588. [PubMed: 21048710]
10. Ludtke SJ, Tran TP, Ngo QT, Moiseenkova-Bell VY, Chiu W, Serysheva II. Flexible architecture of IP_3R1 by cryo-EM. Structure. 2011; 19:1192–1199. [PubMed: 21827954]
11. Amador FJ, Liu S, Ishiyama N, Plevin MJ, Wilson A, Maclennan DH, Ikura M. Crystal structure of type I ryanodine receptor amino-terminal β-trefoil domain reveals a disease-associated mutation "hot spot" loop. Proc. Natl. Acad. Sci. USA. 2009; 106:11040–11044. [PubMed: 19541610]
12. Lobo PA, Van Petegem F. Crystal structures of the N-terminal domains of cardiac and skeletal muscle ryanodine receptors: insights into disease mutations. Structure. 2009; 17:1505–1514. [PubMed: 19913485]
13. Lin CC, Baek K, Lu Z. Apo and $InsP_3$-bound crystal structures of the ligand-binding domain of an $InsP_3$ receptor. Nat. Struct. Mol. Biol. 2011; 18:1172–1174. [PubMed: 21892169]
14. Taylor CW, Tovey SC. IP_3 receptors: toward understanding their activation. Cold Spring Harb. Perspect. Biol. 2010; 2:a004010. [PubMed: 20980441]
15. Anyatonwu G, Joseph SK. Surface accessibility and conformational changes in the N-terminal domain of type I inositol trisphosphate receptors: studies using cysteine substitution mutagenesis. J. Biol. Chem. 2009; 284:8093–8102. [PubMed: 19141613]
16. Tateishi H, Yano M, Mochizuki M, Suetomi T, Ono M, Xu X, Uchinoumi H, Okuda S, Oda T, Kobayashi S, Yamamoto T, Ikeda Y, Ohkusa T, Ikemoto N, Matsuzaki M. Defective domain-domain interactions within the ryanodine receptor as a critical cause of diastolic Ca^{2+} leak in failing hearts. Cardiovasc. Res. 2009; 81:536–545. [PubMed: 18996969]
17. Sureshan KM, Riley AM, Rossi AM, Tovey SC, Dedos SG, Taylor CW, Potter BVL. Activation of IP_3 receptors by synthetic bisphosphate ligands. Chem. Commun. 2009; 14:1204–1206.
18. Chan J, Whitten AE, Jeffries CM, Bosanac I, Mal TK, Ito J, Porumb H, Michikawa T, Mikoshiba K, Trewhella J, Ikura M. Ligand-induced conformational changes via flexible linkers in the amino-terminal region of the inositol 1,4,5-trisphosphate receptor. J. Mol. Biol. 2007; 373:1269–1280. [PubMed: 17915250]
19. Mayer ML. Glutamate receptors at atomic resolution. Nature. 2006; 440:456–462. [PubMed: 16554805]

20. Hamada T, Bannister ML, Ikemoto N. Peptide probe study of the role of interaction between the cytoplasmic and transmembrane domains of the ryanodine receptor in the channel regulation mechanism. Biochemistry. 2007; 46:4272–4279. [PubMed: 17361990]
21. Ramos-Franco J, Galvan D, Mignery GA, Fill M. Location of the permeation pathway in the recombinant type-1 inositol 1,4,5-trisphosphate receptor. J. Gen. Physiol. 1999; 114:243–250. [PubMed: 10436000]
22. Samso M, Feng W, Pessah IN, Allen PD. Coordinated movement of cytoplasmic and transmembrane domains of RyR1 upon gating. PLoS Biol. 2009; 7:e85. [PubMed: 19402748]
23. Iwai M, Michikawa T, Bosanac I, Ikura M, Mikoshiba K. Molecular basis of the isoform-specific ligand-binding affinity of inositol 1,4,5-trisphosphate receptors. J. Biol. Chem. 2007; 282:12755–12764. [PubMed: 17327232]
24. Chu A, Diaz-Munoz M, Hawkes MJ, Brush K, Hamilton SL. Ryanodine as a probe for the functional state of the skeletal muscle sarcoplasmic reticulum calcium release channel. Mol. Pharmacol. 1990; 37:735–741. [PubMed: 1692609]
25. Lai FA, Meissner G. The muscle ryanodine receptor and its intrinsic Ca^{2+} channel activity. J. Bioenerg. Biomembr. 1989; 21:227–246. [PubMed: 2546931]
26. Liu Z, Wang R, Tian X, Zhong X, Gangopadhyay J, Cole R, Ikemoto N, Chen SR, Wagenknecht T. Dynamic, inter-subunit interactions between the N-terminal and central mutation regions of cardiac ryanodine receptor. J. Cell Sci. 2010; 123:1775–1784. [PubMed: 20427316]
27. George CH, Jundi H, Thomas NL, Scoote M, Walters N, Williams AJ, Lai FA. Ryanodine receptor regulation by intramolecular interactions between cytoplasmic and transmembrane domains. Mol. Biol. Cell. 2004; 15:2627–2638. [PubMed: 15047862]
28. Otwinowski Z, Minor W. Processing X-ray diffraction data collected in oscillation mode. Methods Enzymol. 1997; 276:307–326.
29. McCoy AJ, Grosse-Kunstleve RW, Adams PD, Winn MD, Storoni LC, Read RJ. Phaser crystallographic software. J. Appl. Crystallogr. 2007; 40:658–674. [PubMed: 19461840]

References

30. Otsu K, Willard HF, Khanna VK, Zorzato F, Green NM, MacLennan DH. Molecular cloning of cDNA encoding the Ca^{2+} release channel (ryanodine receptor) of rabbit cardiac muscle sarcoplasmic reticulum. J. Biol. Chem. 1990; 265:13472–13483. [PubMed: 2380170]
31. Tovey SC, Dedos SG, Rahman T, Taylor EJA, Pantazaka E, Taylor CW. Regulation of inositol 1,4,5-trisphosphate receptors by cAMP independent of cAMP-dependent protein kinase. J. Biol. Chem. 2010; 285:12979–12989. [PubMed: 20189985]
32. Kenakin, TP. Pharmacologic analysis of drug-receptor interactions. 3rd ed. Lippincott, Williams and Wilkins; New York: 1997.
33. Murshudov GN, Vagin AA, Dodson EJ. Refinement of macromolecular structures by the maximum-likelihood method. Acta Crystallogr D Biol Crystallogr. 1997; 53:240–255. [PubMed: 15299926]
34. Emsley P, Cowtan K. Coot: model-building tools for molecular graphics. Acta Crystallogr D Biol Crystallogr. 2004; 60:2126–2132. [PubMed: 15572765]
35. Zorzato F, Fujii J, Otsu K, Phillips M, Green NM, Lai FA, Meissner G, MacLennan DH. Molecular cloning of cDNA encoding human and rabbit forms of the Ca^{2+} release channel (ryanodine receptor) of skeletal muscle sarcoplasmic reticulum. J. Biol. Chem. 1990; 265:2244–2256. [PubMed: 2298749]
36. Tovey SC, Sun Y, Taylor CW. Rapid functional assays of intracellular Ca^{2+} channels. Nat. Protocol. 2006; 1:259–263.
37. Pettersen EF, Goddard TD, Huang CC, Couch GS, Greenblatt DM, Meng EC, Ferrin TE. UCSF Chimera - a visualization system for exploratory research and analysis. J. Comput. Chem. 2004; 25:1605–1612. [PubMed: 15264254]
38. Wriggers W, Milligan RA, McCammon JA. Situs: a package for docking crystal structures into low-resolution maps from electron microscopy. J. Struct. Biol. 1999; 125:185–195. [PubMed: 10222274]

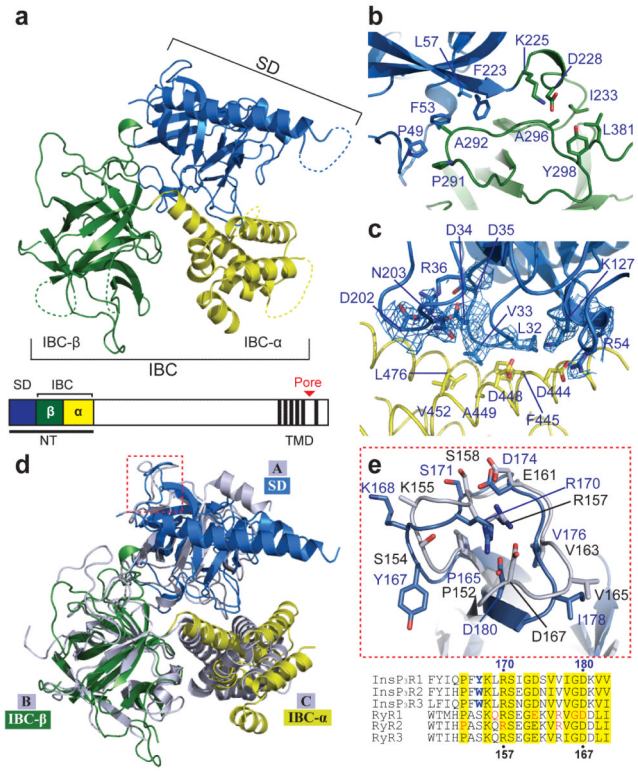

Figure 1. Structure of the N-terminal region of $InsP_3R1$ without $InsP_3$ bound

a, Structure of $NT^{Cysless}$ at 3 Å resolution showing SD (blue), IBC-β (green) and IBC-α (yellow). Dashed lines show invisible regions in electron density. Positions of the three domains within a single $InsP_3R$ subunit are shown. **b**, **c**, Interfaces between SD/IBC-β (β-interface) (**b**) and SD/IBC-α domains (α-interface, with the hydrophobic core boxed and the $2F_o$-F_c electron density map of key residues (contoured at 1.0 σ) shown as mesh) (**c**). **d**, Superposition of apo-$NT^{Cysless}$ and RyR1-ABC (grey)[9] structures by overlaying IBC-β and RyR1 B-domain. 'Hot spot' (HS) loop in RyR1 and corresponding region in $InsP_3R1$ are highlighted (red). **e**, Close-up views of HS regions of $InsP_3R1$ (blue) and RyR1 (grey, black lettering) with conserved residues depicted as sticks. Structure-based DALILite alignment of rat $InsP_3R$ and rabbit RyR show conserved residues in yellow, RyR1 disease-associated mutations in red, and hydrophobic residues implicated in activation of $InsP_3R$ in blue[8].

Europe PMC Funders Author Manuscripts

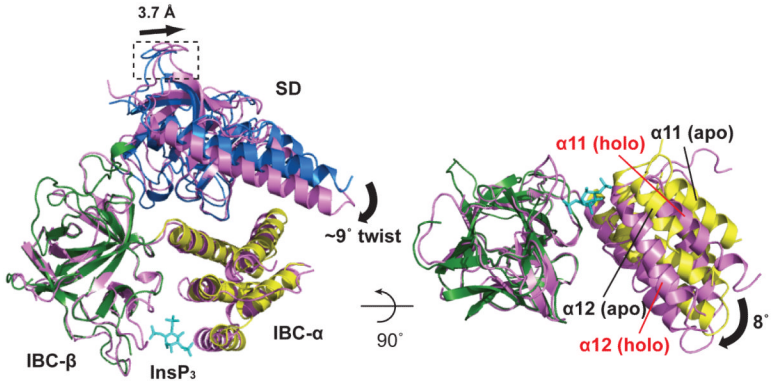

Figure 2. $InsP_3$-evoked conformational changes

Superposition of apo-$NT^{Cysless}$ (SD, blue; IBC-α, yellow; IBC-β, green) and $InsP_3$-bound $NT^{Cysless}$ (3.6 Å resolution, magenta) by overlaying IBC-β domain. $InsP_3$ binding causes the SD to rotate towards the IBC accompanied by a swing approximately perpendicular to the IBC 'clam closure'. This twist (curved arrow) is measured as the angular difference between the SD arm helices in the apo- and bound states (~9°). Movement of the HS-loop (boxed) shows the distance between α-carbons of Y167 (~3.7 Å). A view rotated 90° about the x-axis is shown at right with only IBCs represented. The interdomain (IBC-β and IBC-α) angular difference between the free and bound states is ~8° (black arrow). Further details of $InsP_3$ binding and its effects on the IBC and α- and β-interfaces in Supplementary Figure 5.

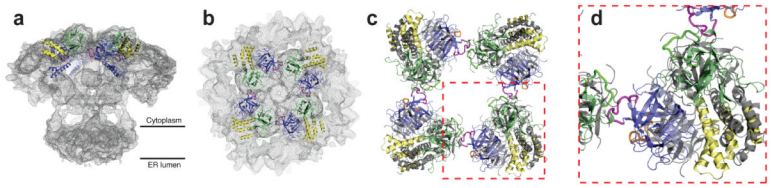

Figure 3. Docking of the apo-NT^{Cysless} structure into the cryo-EM map of InsP$_3$R1

a, **b**, Side (**a**) and top (**b**) views of apo-NT^{Cysless} structure docked into the cryo-EM map (grey mesh) of InsP$_3$R1 in a closed state[10]. Contour level corresponds to mass of InsP$_3$R1 tetramer of 1.3 MDa (protein density 0.8 Da/Å^3). Four molecules of the NT (SD, blue; IBC-β, green; IBC-α, yellow) are located at top of the cytoplasmic portion of the InsP$_3$R1 tetramer. **c**, **d**, Dockings of the apo-NT^{Cysless} (coloured as in a) and ABC[9] (grey) structures into cryo-EM structures of InsP$_3$R1[10] and RyR1[9], respectively, are overlaid and presented to show only N-terminal structures. HS-loops of InsP$_3$R (magenta) and RyR (orange) are highlighted. Enlargement of boxed area (**d**). Locations of other binding sites within NT of InsP$_3$R1 are shown in Supplementary Figure 6.

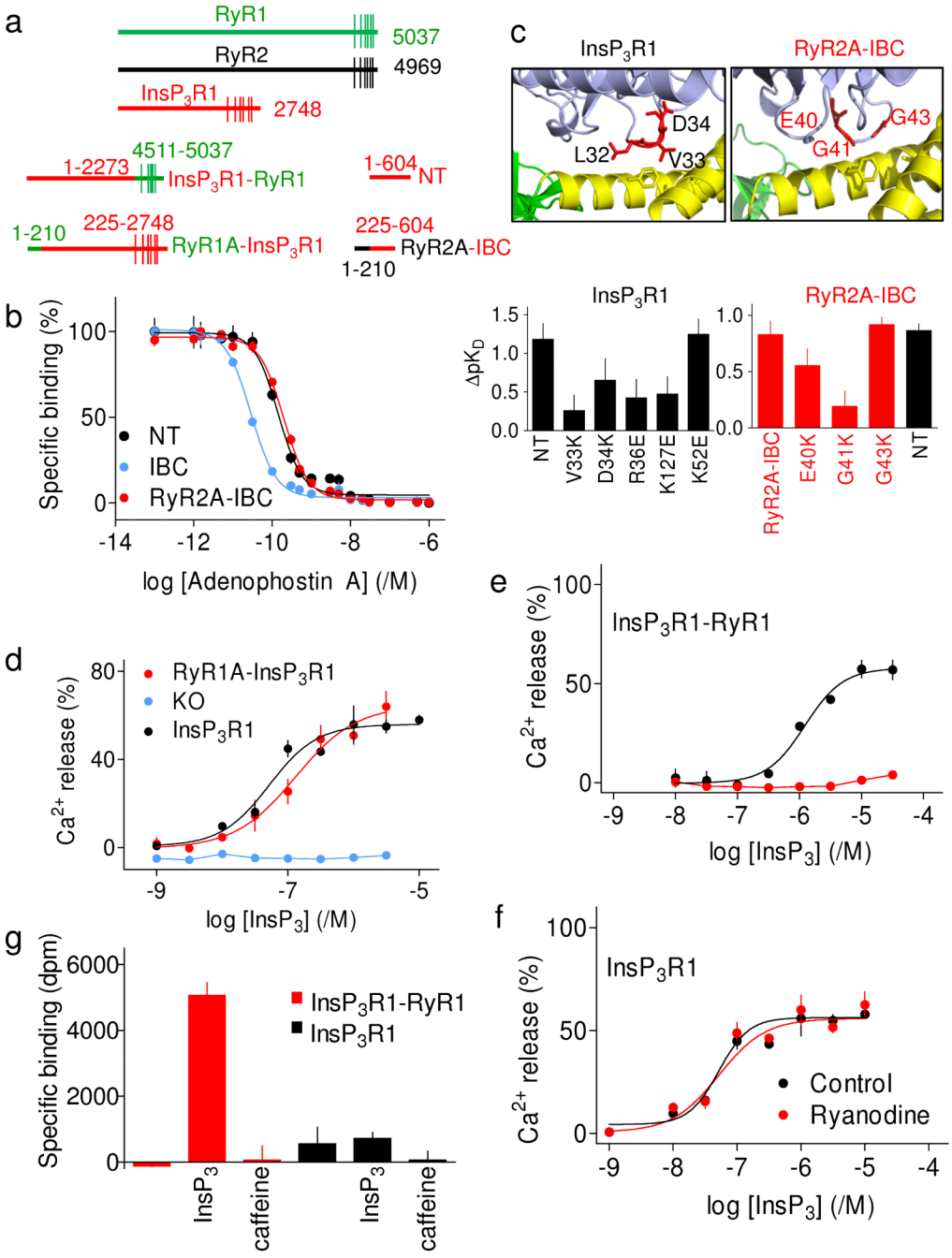

Figure 4. Functional chimeras of $InsP_3R$ and RyR

a, Proteins used. **b**, Specific binding of ^3H-$InsP_3$ in presence of adenophostin A. **c**, Inhibition of ^3H-$InsP_3$ binding to IBC by SD or A-domain, and effects of mutations within equivalent loops. Affinities shown relative to IBC (ΔpK_D). Structures show key residues within SD or A-domain at α-interface. **d**, Ca^{2+} release from DT40 cells expressing $InsP_3R1$, RyR1A-$InsP_3R1$ or lacking $InsP_3R$ (KO). **e**, **f**, Effect of ryanodine (10 μM) on Ca^{2+} release from DT40 cells expressing $InsP_3R1$-RyR1 (**e**) or $InsP_3R1$ (**f**). Ryanodine (≤10 μM) did not stimulate Ca^{2+} release via $InsP_3R1$-RyR1 suggesting that TMDs may not alone mediate stimulation of RyR[25]. Results (**d**-**f**) are percentages of ATP-dependent Ca^{2+} uptake. **g**,

Specific ^{3}H-ryanodine binding (dpm, disintegrations/min) to membranes of DT40 cells expressing $InsP_3R1$ or $InsP_3R1$-RyR1 with caffeine (10 mM) or $InsP_3$ (1 μM). Non-specific binding was 2245 ± 211 dpm. Results (**b**-**g**) are means ± s.e.m., n ≥ 3.

Europe PMC Funders Author Manuscripts